Int. J. Multiphase Flow Vol. 13, No. 4, pp. 459–475, 1987
Printed in Great Britain.

0301-9322/87 $3.00 + 0.00

INSTABILITIES IN SELF-FLUIDIZED BEDS—II

EXPERIMENTS

D. GREEN and G. M. HOMSY
Department of Chemical Engineering, Stanford University, Stanford, CA 94305, U.S.A.

(*Received* 12 *May* 1986; *in revised form* 24 *December* 1986)

Abstract—Experimental studies of the behavior of self-fluidized beds in both 2-D and 3-D are reported. The experimental system used was the drying of silica gel under vacuum, and wide ranges of particle sizes and drying rates were covered. Both flow visualization and dynamical measurements of flow rates were utilized in the study. The observations indicate that self-fluidization is always unstable above the source strength required for minimum fluidization. The instability takes one of two forms, depending upon the degree of supercriticality. The primary instability consists of a quasi-steady array of spatially periodic spouts. A secondary instability leads to the emergence and dominance of larger spouts, which are observed to appear and disappear in a cyclic fashion. Measurements are made of wavelengths of the primary instability and the frequency of the secondary instability as functions of the operating variables, and the secondary instability is seen to occur at the same normalized flow rate for all the particles studied. Plausible mechanisms for these instabilities are proposed and discussed.

1. INTRODUCTION

Under certain conditions, vapor from a bed of drying or degassing granular material can fluidize the upper layers of the bed. This will occur when the velocity of the gas in some region of the bed exerts an upward drag force on the particles which is equal to or greater than the downward force due to gravity. This condition is analogous to that in conventional fluidization, where a fluid is pumped through a distributor into the bottom of a bed of solid particles and flows upward through the bed. When the interstitial gas velocity is sufficiently high, the bed fluidizes.

As the source of fluid in a drying bed is entirely within the bed itself, fluidization resulting from such a source has been called "self-fluidization". A key difference between conventional and self-fluidization is the spatial dependence of the magnitude of the fluid velocity in the bed. The averaged component of the fluid velocity in conventionally fluidized beds is constant in space, but in vertical self-fluidization the fluid velocity increases with increasing height in the bed. Assuming that the strength of the source is uniform, the flux through any horizontal plane in the bed will be proportional to the height of the plane. Therefore, the fluid velocity increases with increasing height in the self-fluidized bed.

It is well-known (Anderson & Jackson 1968; Homsy *et al.* 1980) that conventionally fluidized beds are unstable for all fluid velocities above the minimum necessary to fluidize the bed. For liquid fluidized beds, the form of the instability is found to be planar waves of increased voidage which originate near the distributor and propagate upwards through the bed. These waves develop a transverse structure that leads to the formation of "bubbles" or particle-lean regions which also propagate upwards in a manner analogous to bubbles rising in a liquid (El-Kaissy & Homsy 1976; Didwania & Homsy 1981). Gas fluidized beds have been shown to be 1–2 orders of magnitude less stable than liquid fluidized beds (Anderson & Jackson 1968), and as a result begin to bubble almost immediately upon the onset of fluidization.

Self-fluidized beds are similarly unstable. Jewett & Lawless (1982), in an exploratory study, observed an instability that took the form of spouts of particles erupting from the surface of a bed of drying silica gel. Under certain conditions, these spouts persisted for several minutes. Several spouts were observed at any one time and seemed to occur with a constant spatial frequency. There was no evidence of either the planar voidage waves or bubbling associated with conventional fluidization.

A steady spatially periodic instability was also observed in the current work. This primary instability consisted of an array of spouts at the surface of a bed of drying silica gel in a 2-D

apparatus. In addition, a temporally periodic secondary instability was observed in which a single large spout grew from the initial array and came to dominate the flow in the entire apparatus. The periodicity arose because dominant spouts expire and growth begins anew.

Therefore, self-fluidization presents an instability which is both similar to and different from the instability found in conventionally fluidized beds. Both instabilities consist of fluctuations in the local void fraction. These disturbances take the form of voidage waves and bubbles in conventional fluidization, but are found to be spatially periodic arrays of spouts for self-fluidization.

The limited observations made to date of the self-fluidization instability have raised several questions. Is the flow stable under certain conditions, or is it unconditionally unstable? Are the motions associated with the instability steady or do they evolve over time? How does the instability originate, and, in particular, what is the mechanism for the birth and the growth of these apparently spatially periodic spouts? What are the length and time scales associated with the instability and how do they depend upon the parameters which govern the system?

The work of Jewett & Lawless (1982) was largely descriptive, so there is need for a controlled, quantitative study of the phenomenon. Therefore, the objective of the current experimental study is to observe and measure the flows associated with the instability under controlled and monitored conditions. In particular, the spatial and temporal frequencies of the instabilities have been measured. The mean flow rate of the system was regulated, affording a controlled variation of the strength of the source of fluid within the bed. In this way, the effect of the source strength on the characteristics of the instability could be studied. The effect of particle properties and bed geometry on the characteristics of the instability was also investigated. Finally, a mechanism for the growth of the instability is proposed. This provides the basis for the development of a theoretical investigation which is discussed in a companion paper.

A brief outline of the rest of this paper is as follows. In section 2, the apparatus and instrumentation used in the study are presented along with the measurement and data collection procedures. Results and observations are given in section 3, beginning with a discussion of the range of parameters studied and an overview of the phenomena observed, and continuing with more detailed measurements of minimum fluidization conditions and the spatial and temporal frequencies of the instability. These findings are discussed and a mechanism proposed for the instability in section 4 and the conclusions of the study are summarized in section 5.

2. EQUIPMENT

Apparatus

Most of the data discussed below were obtained in a 2-D flow cell. Experiments were also performed in a 3-D cell in order to verify that the 2-D experiments captured the true nature of the instability. The instrumentation and pumping apparatus remained the same for experiments in 2-D and 3-D. Only the flow cell itself was changed.

A vacuum-tight cell was constructed for the 2-D experiments. A 50 × 20 cm cavity was machined into a solid block of aluminum. The cavity was machined to be 3 cm deep, but the depth could be varied using two spacer plates (thicknesses: 1.6 and 0.79 cm) which were made to fit loosely into the cavity and were attached to the rear wall with machine screws. These spacers were sealed around the edges to prevent gas flow around them. Using these spacers and an assortment of shims, cell depths of 3.0 and 2.2–0.0 cm were possible. In operation, the cell was oriented so that the cavity was 20 cm "high" in the vertical direction. The 50 cm "width" and variable "depth" were then horizontal dimensions. In order to permit visual observation of the flow, a 2.5 cm thick piece of glass was used as one wall of the chamber. The glass fitted into a frame formed by the outer chamber walls and was held in place by two small clamps and was sealed by a combination of a thin neoprene gasket and vacuum grease. As a vacuum was drawn in the chamber, the glass was pulled very tightly onto its frame, providing a reliable seal. In order to minimize stray reflections and increase contrast with the light-colored particles, all aluminum parts of the apparatus were black anodized.

Figure 1 is a schematic diagram of the apparatus. Water vapor from drying silica gel exited the cell from a single port at the top. A dial-type thermometer measured the temperature of the vapor

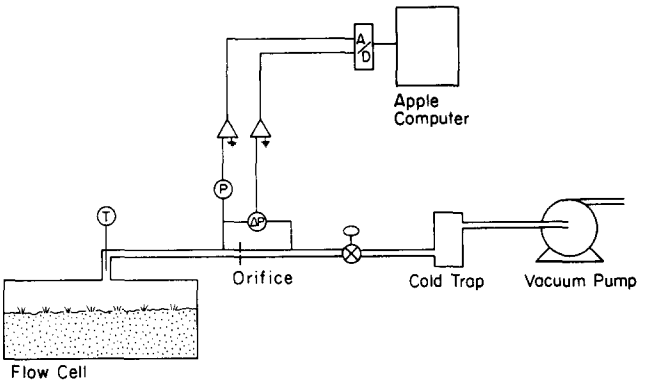

Figure 1. Schematic of the apparatus.

at the port; 2.5 cm o.d. copper tubing was used to conduct the vapor throughout the rest of the apparatus.

The flow rate was measured with an orifice plate flowmeter, and the pressure drop was measured with a Validyne DP215TL transducer. At the upstream pressure tap, the absolute pressure was measured with an MKS Baratron 222BA transducer. All of the tubing from the cell to the globe valve was insulated with aluminum-backed foam wrap. This insured that the effluent from the cell did not change temperature before its flow rate was measured at the orifice flowmeter. Downstream of the flowmeter, a Crane globe valve was used to control the mean flow rate of the vapor exiting the cell. A cold trap and mechanical vacuum pump in series provided the pumping capacity to maintain the flow rates necessary to fluidize the system. In practice, the cold trap provided most of the pumping capacity. During several of the runs with the larger particles, both the exterior and the well of the cold trap were chilled with dry ice in alcohol in order to provide sufficient surface area to condense water at the rate it was produced in fluidizing the bed.

Experiments in 3-D were carried out in a cell consisting of a 25.5 cm high and 14.0 cm dia clear acrylic cylinder with two flat end pieces, also of clear acrylic. These end pieces were connected by four long bolts which, when tightened, held both plates tight against the flat ends of the cylinder. Again, the vacuum in the cell helped to maintain a reliable seal. Being clear, the acrylic cylinder and end pieces afforded visual access to the flow. In order to promote more even temperature distributions in the bed, the outside of the lower portion of the cell was insulated with fiberglass pipewrap.

Particles

Jewett & Lawless (1982) claim that they were able to achieve consistent fluidization in their apparatus only with silica gel particles that had been refluxed for 8 h in 12 N HCl. They used two size ranges of particles, both with wide size distributions, and found qualitatively similar behavior for both. Initially, the particles in the current experiments were treated in the same way as in the previous work, but it was found later that this treatment had little effect upon the nature of the flow and particularly upon the instability. The primary effect that Jewett & Lawless (1982) may have observed was the decrease in mean particle size that resulted from the refluxing with HCl. In fact, such drastic treatment was not necessary to decrease the mean particle size. Merely hydrating the particles in an excess of standing water reduced the particle size, although the change was not as great as that effected by the HCl reflux. The wide range of particle diameters resulting from the hydration process required that the particles be sieved into much narrower size ranges before being used in the experiments. Usually only one, but occasionally two, sieve size ranges were used. The average sizes used in the analysis are a simple mean of the largest and smallest particles of the particular size range used. Due to the cracking phenomenon and the fact that the particles had to be rehydrated after each experiment, the particles were frequently resieved.

The maximum flow rates that could be produced in the apparatus placed the upper limit on the size of particles used in the experiments. It was not possible to reliably fluidize particles larger than

925 μm with the flow rates developed. Carryover of small particles out of the flow cell placed a lower limit on the size of particles that were usable. For particle diameters $<300\ \mu$m, carryover was excessive. Four particle size ranges were used for most of the 2-D experiments: 297–355, 425–500, 600–710 and 850–1000 μm. In the 3-D bed, and occasionally in the 2-D experiments, 250–355 μm particles were used. Immediately preceding an experiment, the bulk density of the particles averaged approx. 0.87 g/cm^3. The density at the end of the experiment, of course, depended on the length of time the experiment was run as well as on the mean flow rate during that time, but a typical value for the bulk density after an experiment was 0.78 g/cm^3. Therefore, the change in density of the solid phase over the course of an experiment was small, on the order of 10%, and can be safely neglected.

As the particles were hygroscopic and were also found to react with common laboratory solvents, the void fraction of the material was hard to measure. An estimate of this value was obtained by saturating the particles with water, then measuring the volume of additional water to fill the void space. The value of the void fraction so obtained is 0.44, which agrees with values typical of granular materials of this type.

Instrumentation and control

In order to meet the objectives of the experiments, the requirements for a system of instrumentation are: (1) to control and record the mean flow rate exiting the system; (2) to measure the wavelength exhibited by the initial stage of the instability; (3) to photographically record system behavior under various conditions; and (4) to identify and measure any temporal frequencies associated with the instability.

The mean flow rate from the system, i.e. the average source strength, was controlled with the valve in the line between the cell and the pumping apparatus. This afforded control over the mean flow only, as fluctuations about the mean were possible and occurred routinely in practice. Under certain conditions the flow rate and the pressure within the cell fluctuated so rapidly that manual data acquisition was insufficient. Therefore, digital data acquisition was employed.

An Apple II Plus computer with a Mountain Computer A/D converter with 8-bit precision was used for data acquisition. Some signal processing was done between the transducers and the A/D converter. Two summing amplifiers were constructed which featured selectable gains. With these amplifiers and variable voltage supplies, the d.c. components of the transducer outputs could be subtracted. The selectable gains allowed the amplification to be tailored to any particular set of experimental parameters in order to achieve the optimum accuracy with 8-bit precision.

The sampling was carried out by a BASIC program calling an assembly language subroutine which ran the A/D converter. The subroutine sampled three channels of the A/D once upon each interrupt produced by a Mountain Computer Clock board. Sampling rates were variable between 0.5 and 2 Hz, selectable with a switch package hardwired to the clock board. Upon each interrupt, the following were sampled: (1) the pressure drop across the orifice; (2) the absolute pressure upstream of the orifice; and (3) an event marker button which was used during certain experiments to mark the presence of large spouts or other events occurring in the bed.

Data sets of 128–1024 sampled points were collected sequentially during an experiment. Usually, the flow was cut off between sampling periods with the globe valve while the data were stored on magnetic disks. From 2–6 data sets were typically recorded during the course of a single experiment.

Measurements of the wavelengths observed in the 2-D bed were made photographically. Still photographs were taken with a Canon 35 mm SLR camera fitted with a Canon 50 mm macro-focusing lens. The glass side of the cell afforded excellent visual access to the flow. A 1 cm square grid was drawn on the inside of the glass, providing a ready reference length on all photographs taken of the bed. The same camera and lens were used to record the 3-D experiments. In this case, the camera was placed slightly above the plane of the upper bed surface and angled downward to view the bed surface.

Measurement of mass and volumetric flow rate was achieved with the orifice flowmeter, and digitally-sampled pressure transducers were employed to measure the rapidly varying instantaneous flow rate. The temperature was monitored manually, as it changed only slowly during the course of an experiment.

In many of our experiments, the flow was not steady, but exhibited large excursions due to a time-dependent secondary instability, to be described below. The following approach was used to determine the frequency of occurrence of the large-scale structures associated with the secondary instability. The status of the event marker button, along with the instantaneous flow rate, was sampled by the computer. This button was depressed when a large spout was present in the bed and released when there were no large spouts. This record was then compared to the record of the flow rate, which showed rather large-amplitude fluctuations superimposed on the mean flow rate. Excellent correlation was found between the presence of a spout in the bed and the occurrence of one of the large-amplitude deviations to the base flow rate. Therefore, it was necessary only to monitor the flow rate in order to determine whether one of the large spouting structures was present. The frequency associated with these structures could then be determined by measuring the frequency of occurrence of the large spikes in the flow rate record.

Range of parameters studied

As mentioned previously, mean particle diameters in these experiments range from 300 to 925 μm. In order to achieve 2-D behavior but avoid bridging or particle packing in the narrow gap between the walls of the apparatus, two bed depths were used. The narrower, 0.60 cm, was generally used with the smaller particle size ranges, while the larger, 1.35 cm, was used with the larger particles. Thus the gap ranged between 20 and 40 particle diameters.

The minimum volumetric flow rates studied correspond to the minimum necessary to fluidize the bed for each particle size range and bed depth. These minimum volumetric flow rates range from 630 cm^3/s for the 300 μm particles with the 0.60 cm bed depth, to 1.5×10^4 cm^3/s for the 925 μm particles and the 1.35 cm depth. Large fluctuations were found in the flow rate, but the highest average achieved was 2.6×10^4 cm^3/s (with the larger depth). The absolute maximum, recorded during a transient peak in the flow rate record, was 2.8×10^4 cm^3/s.

It is useful to normalize the volumetric flow rate, Q, with the minimum volumetric flow rate necessary to fluidize the system. The minimum fluidizing flow rate, Q_{min}, depends on the size of the particles and the cross-sectional area of the bed. Therefore, normalizing the measured flow rate serves to remove the dependence on bed depth from the measurements. Because Q_{min} is large for the large particles and because the maximum flow rates were imposed by the pumping apparatus, a limited range of Q/Q_{min} is available for the larger particles. The highest value of Q/Q_{min} obtained for the 326 μm particles was 8.2, while the highest for the 926 μm particles was approx. 2.0. This means that some of the phenomena which occur at high flow rates were not seen for the largest particles. Table 1 shows the particle size ranges and the maximum normalized flow rate achieved for each. Of course, $Q/Q_{min} = 1$ is the minimum flow rate of interest for each range.

It is convenient to think of the mean flow rate of the system in terms of a "source strength", defined as the volumetric flow rate issuing from a unit volume of the bed. Assuming that this source strength is spatially uniform, it is simply the ratio of the total volumetric flow rate to the bed volume:

$$S = \frac{Q}{V}; \qquad [1]$$

here S is the volumetric source strength, Q is the volumetric flow rate and V is the volume of the bed. The range of source strengths studied is 3–31 s^{-1}.

The static height of the bed was varied from 4 to 18 cm in an effort to determine if this parameter had any effect on the behavior of the system, particularly on the frequencies associated with the formation of large spouts in the bed.

Table 1. Particles used in the experiments

Particle size range (μm)	Mean particle diameter (μm)	Maximum Q/Q_{min}
297–355	326	8.2
425–500	463	6.5
600–710	655	3.4
850–1000	925	2.0

Dimensional analysis indicates that there are dynamical dimensionless parameters which govern the flow. The particle diameter, d_p, is the usual choice for the characteristic length. In this problem the inverse of the source strength, $1/S$, is the obvious choice for the characteristic time. The product of d_pS can then be used as the characteristic velocity.

In the study of fluidization, it is customary to choose the following dimensionless parameters. The first is the Reynolds number, $\mathrm{Re} = \rho_f S d_p^2/\mu_f$, where ρ_f is the fluid density, d_p is the particle diameter and μ_f is the viscosity of the fluid. The Reynolds numbers for these experiments ranged from 2×10^{-4} for minimally fluidizing the 300 μm particles, to 2×10^{-2} for the highest average flow rate achieved with the 925 μm particles. The second parameter that is commonly used is the Froude number, $\mathrm{Fr} = g/S^2 d_p$. Here g is the acceleration due to gravity. Froude numbers in these experiments ranged from 11 to 3.6×10^3. The third dynamical parameter is the density ratio, $R = \rho_f/\rho_s$. The solid density, $\rho_s = 2$ g/cm^3 and $\rho_f = O(10^{-6})$; therefore, $R \ll 1$, and is not expected to have a large effect on the characteristics of the flow.

3. RESULTS

Overview of observed phenomena

Before presenting detailed results, it is useful to give an overview of the motions observed as the volumetric flow rate, Q, is increased above $Q_{\min}$.

Instability occurred at all flow rates studied, including the minimum necessary to fluidize the bed. Fluidization first became evident at discrete sites on the bed surface which began to erupt slightly. These motions were suggestive of very small intermittent spouts. At slightly higher flows, the entire bed surface was fluidized, and small spouts of particles pushed above the bed surface were observed to occur with a relatively constant spacing along the surface of the bed in the 2-D apparatus. Figures 2a–c are photographs of this phenomena for a range of particle sizes. This behavior persisted for flow rates from 1.0 to about 2.5 times the minimum fluidizing flow rate. The spouts were free to move on the surface of the bed, but tended to maintain the same spacing. This form of the instability can be characterized as nearly steady, spatially periodic and 2-D, and will subsequently be referred to as the "primary instability'. The spatial frequency of this flow was found to depend on the operating conditions of the system.

Above approx. 2.5 times the minimum fluidizing flow rate, a much more complicated behavior began as a secondary instability became evident. This occurred when one or several of the small spouts began to grow at the expense of their neighbors as fluid from the surrounding portions of the bed channeled into them. One of these spouts would then continue to grow, again at the expense of its neighbors, until it dominated the entire bed, with most of the fluid flow then channeling into it. Figures 3a, b show a few steps in the evolution of this spouted structure with its associated umbrella-shaped plume of particles. Note that the rest of the bed surface was quiescent.

These large spouts, however, did not persist. They tended to abruptly die out several seconds after attaining their full size. The bed then became quiescent for a short interval (2–10 s). The bed surface then leveled and the bed refluidized, again exhibiting the small spouting behavior characteristic of the primary instability. Shortly, the entire sequence began anew as several of the small spouts began growing until one finally dominated the entire bed again. The motion is therefore cyclic at higher flow rates, starting and returning to the same form of the instability observed at lower flow rates, but with an intermediate, more agitated phase of secondary instability. The system was found to cycle between the two stages of the instability with a characteristic temporal frequency. This time-dependent behavior and the associated motion are referred to subsequently as the "secondary instability".

The same type of behavior was found in the 3-D experiments, except that more than one mature large spout could exist in the system at any one time. Also, the smaller spouts, still with a relatively constant spacing, appeared in small patches on the bed surface rather than in a linear array as they must in the 2-D apparatus.

As both the 2-D and 3-D experiments were run, there was a gradual decrease in the mean flow rate, corresponding to the gradual cooling of the particles in the bed. Typically, however, an experiment can be run for 0.5 h or more, so the decay in flow rate over time is gradual, and the experiments can be considered to be quasi-steady.

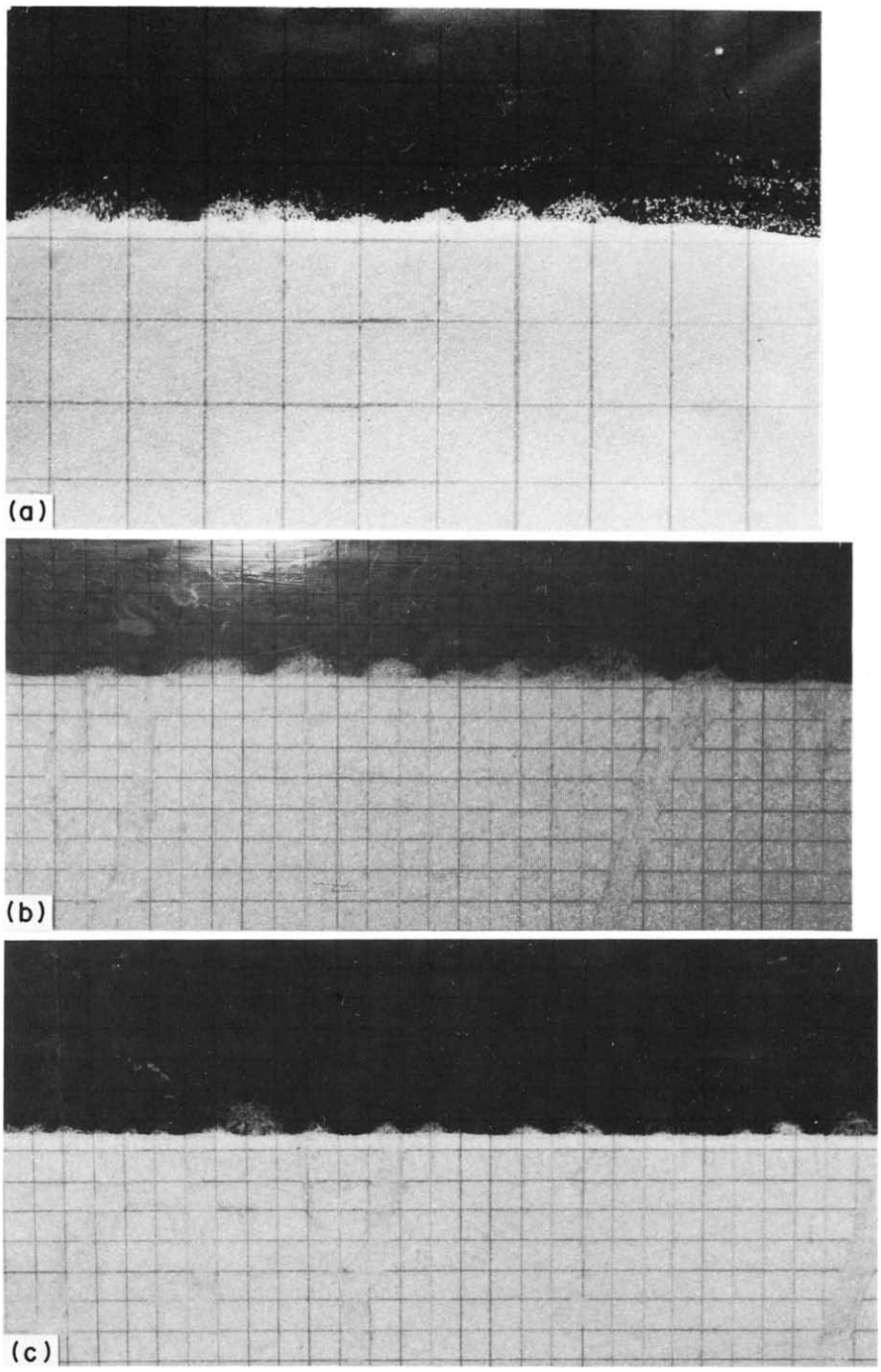

Figure 2. Flow visualizations of the primary instability: (a) $d_p = 326\ \mu m$; (b) $d_p = 463\ \mu m$; (c) $d_p = 655\ \mu m$.

Experiments in 2-D

Conditions for minimum fluidization

Since the fluid velocity in a bed fluidized from a uniform internal source increases with increasing height in the bed, conceptually there will be a "plane of minimum fluidization" above which velocities are greater than the minimum fluidizing velocity. Below this plane there is flow through a packed section. In fact, this plane is not clearly observable: first, it is difficult to discern just where fluidization begins and packed-bed behavior ends, and secondly, much of the excess gas flow (above that necessary to minimally fluidize the bed) is channeled into the spouting structures of the instability.

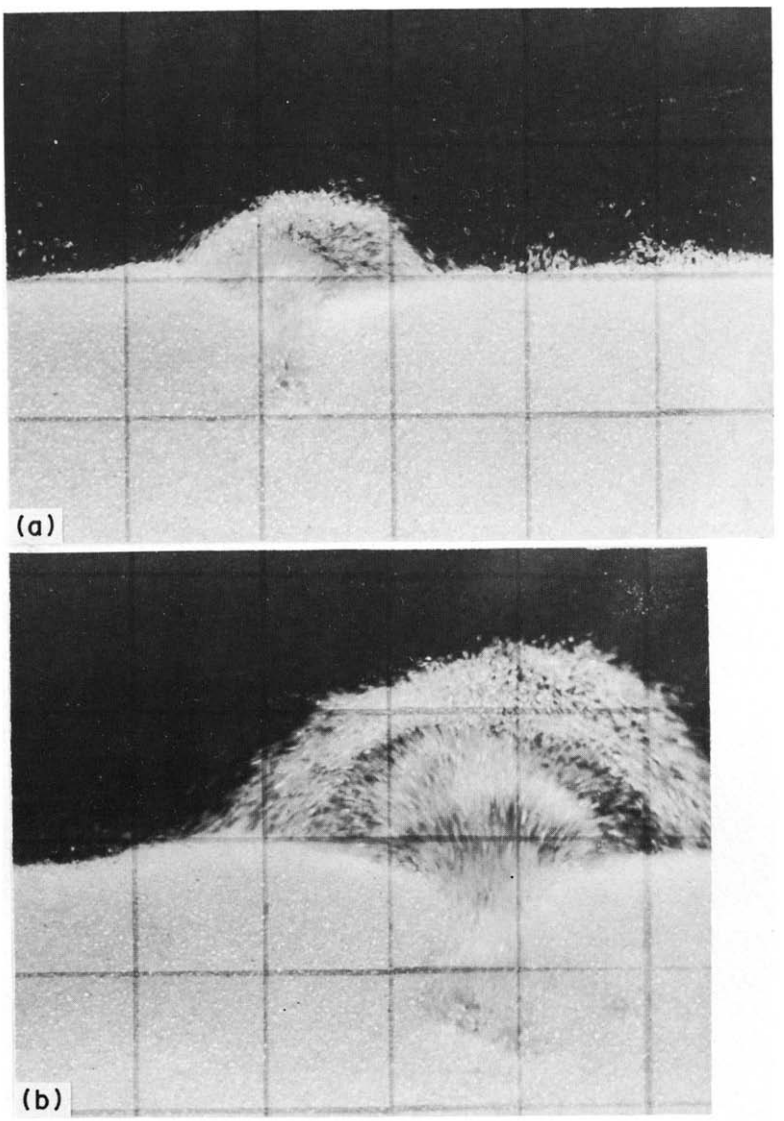

Figure 3. Evolution of the secondary instability for the 326 μm particles.

At the conditions for minimum fluidization, the plane of minimum fluidization coincides with the upper surface of the bed. The flow through the bed is that of flow through a packed section, except for an infinitesimally thin layer at the bed surface which is fluidized. This is a difficult condition to detect, but visual observation was used here to identify the transition because bed pressure drop or other methods commonly used to identify the onset of fluidization were difficult to implement in this vacuum system. The flow rate was increased slowly from below the value where fluidization first begins until fluidization was judged to first occur at the bed surface. This minimum fluidizing flow rate was measured for four different particle sizes, and the results, expressed as superficial velocities, are tabulated in table 2. The values measured ranged from 25 cm/s for particles of 326 μm mean particle diameter to 220 cm/s for 925 μm particles.

As expected, the minimum flow rate necessary to fluidize the bed increases with increasing particle size. Also, a definite hysteresis was observed similar to that in conventionally fluidized beds. This hysteresis was observed for all but the largest, 925 μm, particles.

A comparison with established relations for the minimum fluidizing velocity of conventionally fluidized beds was performed. Under conditions of minimum fluidization, the fluid flow through

Table 2. Observed and predicted minimum fluidizing velocities

Mean particle size (μm)	*Minimum fluidizing velocity at the surface (cm/s)* Observed: Unfluidized–fluidized	Observed: Fluidized–unfluidized	Predicted	Ratio: Observed/Predicted: Unfluidized–fluidized	Ratio: Observed/Predicted: Fluidized–unfluidized
326	25.1	21.0	21.6	1.2	1.0
463	56.9	43.6	43.7	1.3	1.0
655	103.0	74.5	87.3	1.2	0.9
925	220.0	226.0	173.0	1.3	1.3

the bed just supports the weight of the particles. In the usual way, the Ergun equation (Grace 1982), which predicts the pressure drop in packed beds, was used to predict the pressure which was then equated to the weight of the particles. The following relation results:

$$\mathrm{Re}_{\mathrm{mf}} = [C_1^2 + C_2\,\mathrm{Ga}]^{\frac{1}{2}} - C_1, \qquad [2]$$

where

$$\mathrm{Re}_{\mathrm{mf}} = \frac{\rho_{\mathrm{f}} u_{\mathrm{mf}} d_{\mathrm{p}}}{\mu_{\mathrm{f}}}, \quad \mathrm{Ga} = \frac{\rho_{\mathrm{f}}(\rho_{\mathrm{s}} - \rho_{\mathrm{f}}) g d_{\mathrm{p}}^3}{\mu_{\mathrm{f}}^2}, \quad C_1 = \frac{150(1-\epsilon)}{3.25} \quad \text{and} \quad C_2 = \frac{\epsilon^3}{1.75};$$

u is the superficial fluid velocity and the subscript "mf" indicates conditions of minimum fluidization. The predictions using $\epsilon = 0.44$ are shown together with the experimental values in table 2. This relation tends to slightly underpredict the observed velocity at minimum fluidization, but the ratio of observed to predicted velocities was approximately constant at 1.2 for the four particle size ranges studied. This underprediction is not surprising given the difficulty in visually assessing the onset of fluidization. Also, the Ergun equation is based on results for spherical particles, while the particles used here are aspherical. Since the shape of the present particles is unknown, they were treated as spheres, which may also contribute to the underprediction. In any event, the values of the minimum source strength are within the range of accuracy of established correlations.

Wavelength of the primary instability

The most striking characteristic of the primary instability is the relatively constant spacing of the spouts observed. An array of small spouts of relatively constant separation is formed at the surface of the bed, as shown in figures 2a–c.

The effect of various parameters of the flow on the wavelength was studied. Photographs such as those in figures 2a–c were analyzed to determine the wavelength. The digitally-sampled event marker was used to mark the instant in the flow rate record when the exposure was made. In this way, the instantaneous flow rate was recorded for each photograph, and a record of the flow rate over time for the interval during which the photographs were taken was also available. The distance between spouts was measured, and all distances less than a certain maximum value established by the experimenter were averaged. This limit was established to discount distances between spouts which are obviously not interacting with each other, as is the case when there is a large separation (several wavelengths) between adjacent spouts, as on the right of the photograph in figure 2a. Also, the possibility of doubling and tripling the fundamental spatial frequency was considered when the average was computed. These are difficult measurements to make, as there is much variation from photograph to photograph, and sometimes even within a single exposure. The degree of noise this lends to the data means that care must be exercised when interpreting trends in the data that are not of a very clear nature.

The wavelength was found to depend on the average size of particles used in the experiments. The wavelength, averaged over many photographs, is tabulated in table 3 as a function of the particle size ranges used in the investigation. The trend here is quite clear: the wavelength of the instability increases as the mean particle size increases. In figures 4–6, this wavelength is plotted vs the mean flow rate for various particle sizes. Here the situation is not so clear. The data for particles of mean dia 655 μm shown in figure 4 indicate a trend with the wavelength increasing as the flow rate increases. However, the data for the smaller particles in figures 5 and 6 do not

Table 3. Wavelength of the primary instability

Mean particle size (μm)	Wavelength (cm)
326	0.9
463	1.4
655	1.8

show this so clearly. The trend in the latter plots, if present, may be obscured by the noise in the data.

The data in figures 4 and 6 were collected at two different cell depths, 0.556 and 1.39 cm. These depths correspond to 8.5 and 21 particle diameters and 17 and 43 particle diameters, respectively. Little difference was found between the two different bed depths; certainly any difference is well within the scatter of the data. Therefore, the results do not depend upon the cell depth chosen for these particles. It is believed that the phenomenon was not sensitive to cell depth as long as bridging between the walls of the apparatus was not observed and this evidence supports that belief. Thus the data may be considered accurate descriptions of the behavior of a continuum 2-D motion.

Temporal periodicity of the secondary instability

The secondary instability cycles through several stages, the flow generally becoming stronger and the associated spouting structures larger until the structure breaks down and the instability dies out momentarily. The periodicity this imposes on the flow was studied and the effect of various flow parameters on the associated time scale was investigated.

As mentioned above, there is a very clear correlation between the presence of a large spout in the bed and a large-amplitude spike in the flow rate record. Figures 7a, b show a typical record of the flow rate, normalized with the minimum fluidizing flow rate, as a function of time. The data shown are for the 297–355 μm particles, but the behavior is typical of all the particles studied. These data were digitally sampled at 1 Hz.

The average flow rate decreases with time as the bed cools. Superimposed on the time-varying base flow rate are the large-amplitude spikes associated with the spouting due to the secondary instability. The flow is dominated by the frequency with which the bed cycles through the stages of the instability.

This type of behavior, however, is observed only for flow rates above a certain minimum, which is found to be about 2–3 times the flow rate required for minimum fluidization. In figure 7b, the behavior of the system is shown as it passes through the transition between the primary and secondary instabilities. As the normalized base flow rate drops from about 5 to 2.5, the large spikes associated with the secondary instability occur less frequently, then abruptly die out at $Q/Q_{min} = 3$ (in this case). The flow rate below this transition is much more steady, characterized by very small perturbations to the base flow rate. In this regime, the bed is still fluidized and still unstable, except that here the instability is limited to the smaller, spatially periodic spouts of the primary instability.

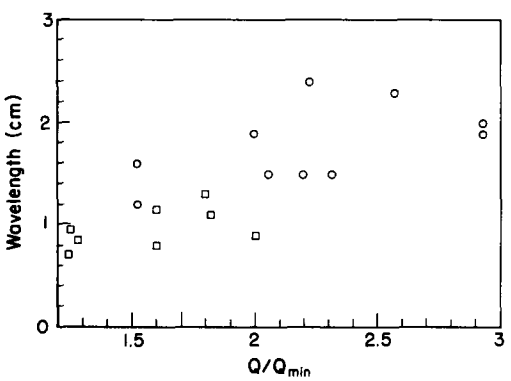

Figure 4. Wavelength of the primary instability vs normalized flow rate, $d_p = 655\ \mu$m: □, gap = 0.56 cm; ○, gap = 1.4 cm.

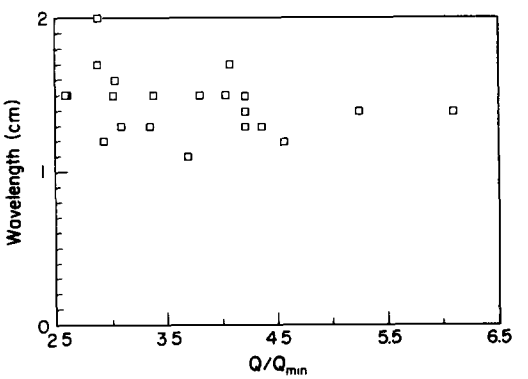

Figure 5. Wavelength of the primary instability vs normalized flow rate, $d_p = 463\ \mu$m: symbols as in figure 4.

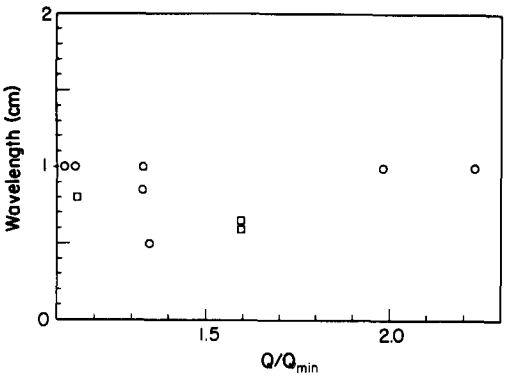

Figure 6. Wavelength of the primary instability vs normalized flow rate, $d_p = 326\,\mu$m: symbols as in figure 4.

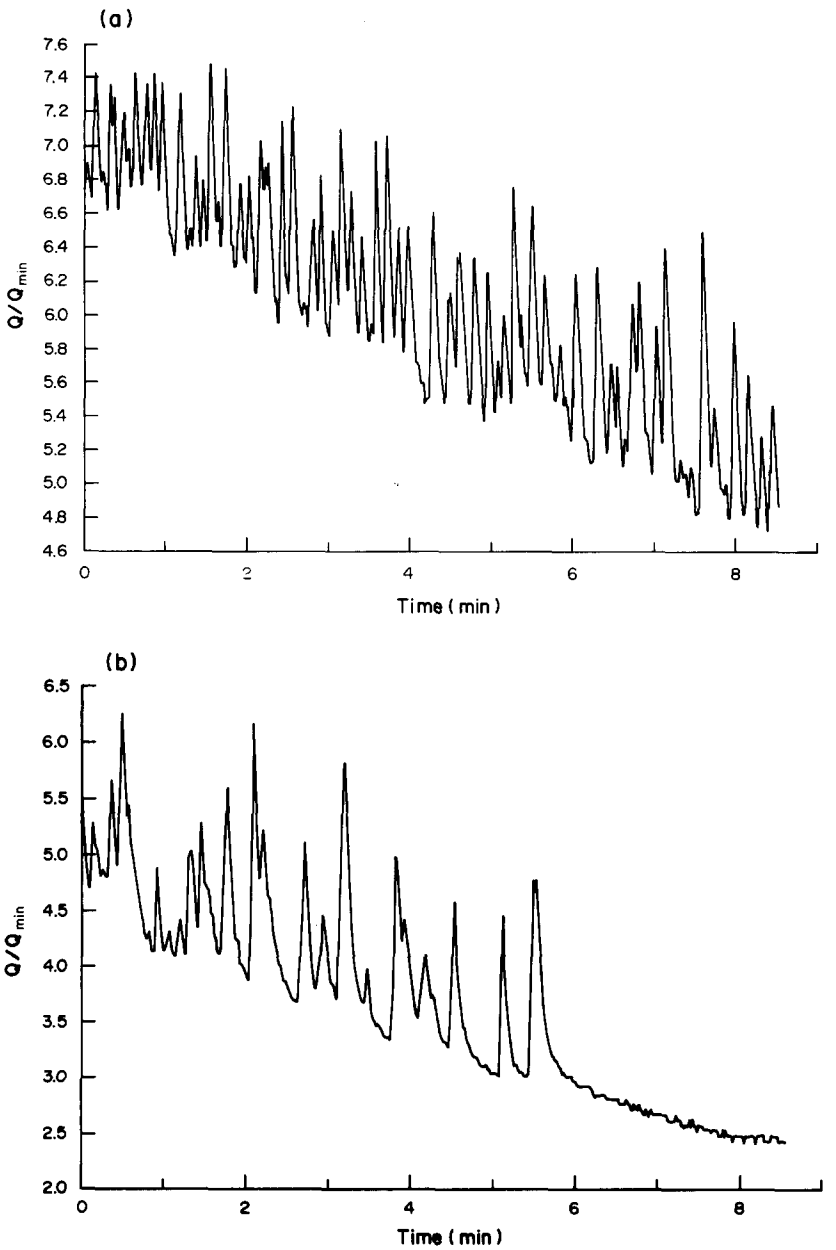

Figure 7. Normalized flow rate vs time.

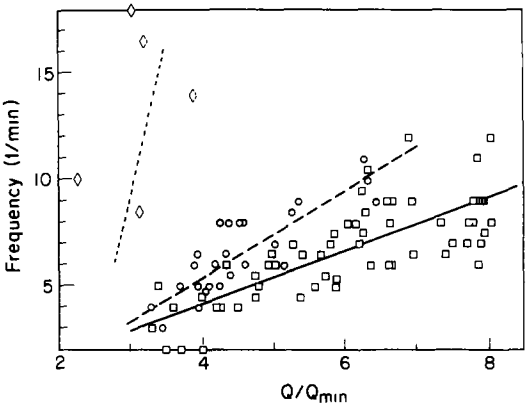

Figure 8. Frequency of the secondary instability vs normalized flow rate: □, $d_p = 326\ \mu$m; ○, $d_p = 463\ \mu$m; ◇, $d_p = 655\ \mu$m.

As shown in table 4, there seems to be no clear dependence of this normalized transition flow rate on any of the parameters studied. That is, no dependence on particle size or static height was found. There may, however, be an effect when the depth of the 2-D cell was changed. This effect is seen in the data for the smallest particles, which were taken with two bed depths. This may be due to the destabilizing effect of the enhanced heat transfer provided by the closer chamber walls of the smaller gap, which we will discuss below.

The frequency associated with the secondary instability does show a dependence on the process parameters. Figure 8 shows the frequency of occurrence of large spouts as a function of the normalized flow rate. The frequencies shown were determined by counting the number of spikes per unit time on the flow rate record. The values obtained were compared with the results of a digital Fourier analysis for several cases, and the frequencies found by both methods agreed. The measured frequency was observed to increase as the flow rate increased for every particle size studied.

The data suggest that the effect of particle size is to change the slope of the line of frequency vs volumetric flow rate. The line of least slope is for the smallest particles studied, those in the range of 297–355 μm. The slope increases with particle size and is at a maximum for the 655 μm particles, which were the largest particles for which data could be obtained. The 925 μm particles did not exhibit the secondary instability because the maximum flow rate obtainable ($Q/Q_{min} = 2$) was less than the transition flow rate. It should be noted that limited data were available even for the 655 μm particles, due to the limited maximum flow rates that were obtained in the apparatus.

From this study of the advanced stages of the instability, the secondary instability was found to occur only at flow rates $\gtrsim 2.5$ times the observed minimum fluidizing flow rate, and that this normalized transition flow rate was virtually the same for all the particles studied. Also, it was observed that the large spouts associated with the secondary instability occur more frequently as the average volumetric flow rate through the system is increased. The dependence of frequency on flow rate is observed to be more pronounced for the larger particles studied.

Experiments in 3-D

Experiments in a 3-D flow cell were undertaken in order to verify that the phenomena observed in 2-D are similar to those found for self-fluidization in 3-D. The type and size of particles,

Table 4. Transition between the primary and secondary instabilities

Mean particle size (μm)	Q/Q_{min} at transition, Bed depth (cm) 0.6	1.4
326	1.8	2.9
463		3.2
655		2.5

normalized flow rates and pressures were all similar to those used in the 2-D experiments. The only difference was the geometry of the cell containing the bed of particles.

The observed behavior was qualitatively similar to the flow in the 2-D cell, although some differences were noted. Photographs of the flow are shown in figures 9a–c. These show the instability in various stages of development in 3-D. The particles in this particular experiment are 250–355 μm. The lighting is from two photoflood lamps to the left of the apparatus and just above the plane of the bed surface. This strong side lighting accentuates the perturbations in the bed surface which result from the instability.

As the system fluidized, the initial stage of the instability was characterized by clusters of small spouts, the numerous small "bumps" in the center of figure 9a. Measurement of the spacing between these spouts on the 2-D surface in these experiments was difficult because of the oblique camera angle, but was roughly the same as the spacing observed in the 1-D array of the 2-D experiments, i.e. on the order of 1 cm. These small spouts persisted for only a short period before one or more grew into larger spouts, very similar to the progression of the instability in 2-D. There was also a small range of flow rates for which these small clusters of spouts persisted without growing into larger spouts. The flow cycled through stages of instability as it did in the 2-D experiments. Large spouts grew at the expense of smaller spouts and eventually dominated large parts of the bed. The large spouts tend to be longer lived, but do die out eventually, leading to the regeneration of the smaller initial spouts. Figures 9b and 9c show spouts at various stages of development. Some spouts become even larger than those shown in figure 9a.

One of the principal differences between 2-D and 3-D flow is the greater likelihood that more than one mature large spout exists in the bed at any one time. This was a very infrequent occurrence in 2-D, but was common in the 3-D cell. In figure 9b, spouts at several stages of development are observed at one time in the cell. There seemed to be no preference of location for the spouts. The form of a particular spout, away from the influence of the walls, exhibited a great degree of radial symmetry. From above, the spout looked like a uniform hole in the bed surface from which a fine spray of particles issued into the freeboard.

The periodicity that the cycling through the stages of the instability imposed on the flow was quite different from that observed in 2-D because there was the possibility of more than one large spout growing and persisting in the bed at any one time. The flow rate was therefore much less periodic in time. There was no one dominant frequency, such as the one associated with the growth, dominance and expiration of single spouts in 2-D.

4. DISCUSSION

In an effort to understand the primary instability which has been observed for self-fluidization, a mechanism is proposed for the initiation and growth of the instability. Any mechanism must explain the origination of the spouting phenomenon and the spatial frequency of the instability that is observed. Furthermore, the mechanism should account for the differences between the mode of instability observed here and those in conventionally fluidized beds.

Consider the presence of random infinitesimal perturbations in the void fraction in the fluidized section of the bed. Any local increase in the void fraction will serve to increase the permeability of the area involved, or equivalently lower the resistance to gas flow, thereby presenting a decreased pressure drop to the local interstitial flow. This causes the velocity of the gas to increase in the region of increased void fraction as more fluid channels into that area from beneath and from the sides. The increase in gas flow will increase the drag force on the particles, and tend to further expand the area experiencing it, thereby further increasing the voidage and causing still more gas to flow into the area. In this way, small perturbations in the void fraction grow due to the increase in local gas flow that they cause. Because of this growth, the flow is unstable and infinitesimal perturbations in the void fraction grow into observable spouting structures. It is believed that this basic mechanism is responsible for the formation of the spouts of the primary instability.

Central to this mechanism of instability is the link between flow in the upper fluidized layer and in the lower packed layer of the bed. Disturbances in the voidage in the fluidized section alter the pressure field in the bed which affects the flow in the lower packed section. Local decreases in the

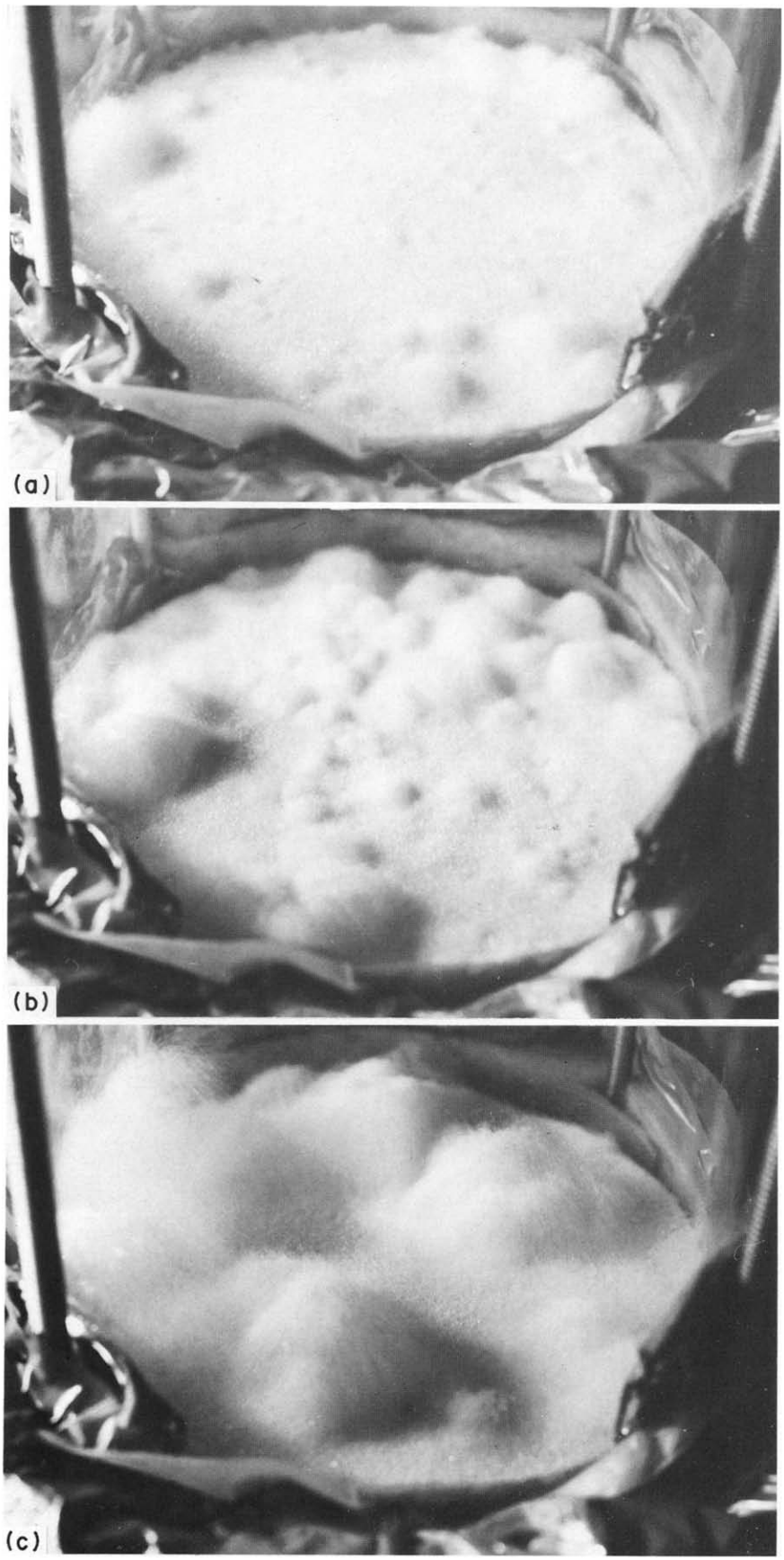

Figure 9. Flow visualizations in the 3-D apparatus: (a) small spouts of the primary instability; (b, c) evolution of the secondary instability.

pressure drop in the fluidized section due to the growing instability will cause the fluid from the packed section to flow *preferentially* into the area experiencing an increase in voidage. This non-uniformity in the flow further amplifies the instability occurring in the fluidized region. This connection in flow between the layers of the self-fluidized bed is important in the development of the primary instability and may also be responsible for the preferential growth of a single spout which characterizes the secondary instability. This is discussed in more detail below.

The most striking characteristic of the primary instability is the relatively constant spacing of the spouts. The mechanism, as outlined above, is non-dissipative. All perturbations in the voidage are amplified, but small wavelengths are preferred. This is because of two effects which enhance the growth of disturbances at small wavelengths. First, the pressure drop which the fluid must overcome in order to channel into a spout will increase as the separation between the spouts increases. Also, spouting requires the establishment of particle circulation within the fluidized layer in order to satisfy continuity. This circulation will occur in cells whose mean horizontal dimension will be roughly one-half of the wavelength. Therefore, the momentum asssociated with this induced circulation also increases as the wavelength increases. In order to minimize the energy losses due to pressure drop related to channeling in the fluid phase and inertial effects related to the circulation of the particles, small wavelengths will be preferred.

Dissipation which damps the growth of disturbances at small wavelengths can cause the development of the constant spatial frequency that is observed. In this case, the viscous-like resistance to shear of the fluidized layer may provide the necessary dissipation. Large separations between spouts produce much less shear and hence less viscous dissipation of energy; therefore, longer wavelengths are preferred. These competing effects, the pressure field/particle inertia which favors the growth of disturbances at small wavelengths and viscous damping which favors the growth of long wavelengths, create the preferred spatial frequency that is observed.

A theoretical investigation based on this mechanism and including the effect of viscous interactions in the flow has been completed and the results are presented in the companion paper (Green & Homsy 1987). This further investigation was undertaken, in part, to better understand the mechanism by which the spatial frequency of this stage of the instability is established.

It was observed experimentally that the primary instability was itself unstable for values of $Q/Q_{\min} > 2$–3. At these higher flow rates, a secondary instability consisting of the growth of some spouts at the expense of their neighbors occurred. Jewett & Lawless (1982) did not observe this secondary instability. They did not record flow rate information, but it seems likely that flow rates in their experiments were always less than the minimum necessary for transition to the secondary flow.

This behavior can be understood by extending the mechanism proposed for the establishment of the primary instability to an array of spouts. Since any region of increased voidage is rendered unstable by the mechanism, the spouts of the primary instability are themselves unstable and tend to grow. Because of the link between disturbances in the fluidized layer and flow in the packed section, growing disturbances are able to affect larger and larger portions of the bed. The growth of any spout that becomes even slightly larger than its neighbors will be favored as more fluid channels into it from both the spouted and the unspouted layers. As a larger spout grows, more and more of the flow from beneath will find its way into the preferred spout and the flow into its immediate neighbors will decrease. Consequently, these neighbors will die out as the growing spout becomes larger. In this way, the initial array of small spouts is disrupted as several spouts become larger and dominate the flow in their immediate neighborhood. These spouts are subject to the same process, and the growth of the larger of these will be favored. Therefore, the mechanism of the formation of the secondary instability is related to that which produces the initial instability.

These large spouts, however, do not persist. They grow to dominate the bed and then die out. Local cooling due to locally increased evaporation rates or drying of the particles may decrease the flow into the large spout, causing it to die out. Because there is no noticeable effect on the location and configuration of the spouting structures due to the previous presence of a large spout at a particular location, the effect that leads to the expiration of a large spout must have a rapid relaxation time. This points to local cooling as the factor most likely to cause this collapse. Heat transfer within the bed, as well as mixing when the spout collapses, may smooth out the temperature gradients resulting from increased rates of water vapor evolution in the neighborhood

of a large spout. Thus, in the length of time it takes the bed to refluidize and reestablish the instability, little or no effect of the preexistence of a large spout is observed.

The growth and expiration of the large structures associated with the secondary instability impose a temporal periodicity on the flow. This characteristic frequency was measured in the experiments and was found to depend on both particle diameter and source strength.

The factors affecting the temporal frequency of the secondary instability can be divided into two classes: those related to the rate of growth of a spout to dominance in the cell, and those that determine when it expires.

The rate of growth of a dominant spout from the quiescent state preceding the establishment of the initial instability through its ultimate form is largely determined by the fluid flow rates involved, i.e. the source strength. At higher flow rates, more energy is available to the instability and its development is accelerated and the observed frequency is increased.

The lifetime of a dominant spout will also affect the observed frequency of occurrence. Dominant spouts were observed to collapse and die out rather abruptly in the experiments, so this may or may not have a large effect on the measured frequency, depending on the extent to which any mechanism which causes the expiration of a spout also slows its growth. The configuration of the apparatus definitely plays a role in determining the lifetime and the degree of dominance of a particular spout. In the 2-D experiments, single spouts were observed to reach dominance while in the 3-D experiments, two or three dominant spouts were frequently found to coexist and to remain active longer than their counterparts in 2-D.

Experimentally, it was found that the frequency associated with the secondary instability decreased as the source strength decreased. This is in agreement with faster growth through the stages of the instability with an increased source strength. From the data collected, however, it is impossible to determine to what extent the mechanism precipitating the death of a spout affects the measured frequency.

Heat transfer may also play a role in the delayed onset of the secondary instability, which was only found to occur above $Q/Q_{\min} = 2.5$ in most of the systems studied. Temperature gradients set up by the initial spouting tend to limit the growth of the spouts, because cooling in the neighborhood of a spout tends to locally lower the source strength. Therefore, heat transfer, which tends to diminish these stabilizing temperature gradients, is a destabilizing effect. The fluid mechanical instability does not become strong enough to drive the secondary instability until $Q/Q_{\min}$ exceeds about 2.5. Anything that enhances the heat transfer would result in a lower flow rate for transition to the regime experiencing the second stage of the instability. This is what was observed in the experiments with 297–355 μm particles. For a gap width of 1.39 cm, the normalized flow-rate for this transition occurred at a normalized flow rate of 2.9, but the data for the 0.56 cm gap indicate that the transition occurred at a much lower flow rate, about 1.8. It is likely that this reduction in the transition flow rate is the result of the increased heat transfer from the walls of the apparatus that occurs for the narrower gap.

5. CONCLUSIONS

It has been observed that a bed of particles, fluidized by the action of water vapor desorbing from their surfaces, is unstable for all values of the parameters which were studied. This instability began with the onset of fluidization and persisted, although with a different nature, up to the highest flow rates achievable with the current experimental apparatus.

The conditions of minimum fluidization were found to be reasonably well-predicted with the Ergun equation, using a void fraction of 0.44.

Experiments in a quasi-2-D flow cell found that the instability occurs in two stages. First, a series of small, steady spatially periodic spouts were observed to form at the surface of the bed. The spatial frequency of the instability was found to increase with increasing particle diameter. The dependence of this wavelength on the source strength is not clear, but the data suggest that the wavelength increases weakly if at all with the source strength. This primary instability was superseded by a temporally periodic secondary instability at higher volumetric flow rates ($Q/Q_{\min} > 2$–3). This secondary instability was characterized by the growth of one of the small spouts of the primary instability into a large structure which dominated the flow in the entire system

until its death a few seconds after reaching its ultimate size. The growth and death of these large spouts imposed a dominant frequency on the mean flow rate exiting the system. This frequency was found to increase with increasing mean flow rate, and the rate of its increase with flow rate increased with increasing particle size over the range studied.

Experiments were also performed in a 3-D flow cell. These showed that the nature of the flow and its instability in 3-D were very similar to that in the 2-D flow cell in which most of the quantitative data were collected. Qualitatively, the instability became evident in the same way as in the 2-D experiments: spouts pushed above the mean bed surface by a locally increased gas flow. The length scale associated with the primary instability was similar to its counterpart in 2-D. A secondary instability was also observed, where a single spout grew to become large and dominate a significant fraction of the bed. It was more likely, however, for more than one mature spout to exist in the cell at any one time than in the previous 2-D experiments.

A mechanism is proposed for the growth of infinitesimal perturbations to the local void fraction into the macroscopic spouting structures that characterized the primary instability in the experiments. This mechanism qualitatively explains the preferential wavelength that is observed as the combination of two competing effects: the perturbed pressure field and particle inertia favoring the growth of disturbances at short wavelengths and viscous effects in the fluidized emulsion damping short wavelengths. A more detailed theoretical investigation of this proposed mechanism is given in the companion paper (Green & Homsy 1987).

The mechanism responsible for the primary instability is extended to an array of spouts and it is argued that an array of disturbances is itself unstable, leading to the observed form of the secondary instability. It is postulated that the expiration of the large spouts is due to local cooling in the vicinity of a spout as it reaches its ultimate form.

Acknowledgements—We wish to acknowledge the U.S. Department of Energy and the Multiphase Processing Program of the NSF for support of this work.

REFERENCES

ANDERSON, T. B. & JACKSON, R. 1968 Fluid mechanical description of fluidized beds. *Ind. Engng Chem. Fundam.* **7**, 12–21.

DIDWANIA, A. K. & HOMSY, G. M. 1981 Flow regimes and flow transitions in liquid fluidized beds. *Int. J. Multiphase Flow* **7**, 563–579.

EL-KAISSY, M. M. & HOMSY, G. M. 1976 Instability waves and the origin of bubbles in fluidized beds. *Int. J. Multiphase Flow* **2**, 379–395.

GRACE, J. R. 1982 Fluidized bed hydrodynamics. In *Handbook of Multiphase Flow* (Edited by HETSRONI, G.). Hemisphere, Washington, D.C.

GREEN, D. & HOMSY, G. M. 1987 Instabilities in self-fluidized beds—I. Theory. *Int. J. Multiphase Flow* **13**, 443–458.

HOMSY, G. M., EL-KAISSY, M. M. & DIDWANIA, A. 1980 Instability waves and the origin of bubbles in fluidized beds—II. *Int. J. Multiphase Flow* **6**, 305–318.

JEWETT, D. M. & LAWLESS, J. G. 1982 Spouts in a bed of silica powder associated with fluidization by outgassing of adsorbed water. *Int. J. Multiphase Flow* **8**, 439–442.